



Microstructure characterization of electric field assisted sintering (EFAS) sintered metallic and ceramic materials using local thermal diffusivity measurement

Changing the World's Energy Future

Zilong Hua, Jorgen Fredrick Rufner, Arin Seth Preston, David H Hurley,
Patrick Merighe, Spencer Doran, Robert Schley, Yuzhou Wang



DISCLAIMER

This information was prepared as an account of work sponsored by an agency of the U.S. Government. Neither the U.S. Government nor any agency thereof, nor any of their employees, makes any warranty, expressed or implied, or assumes any legal liability or responsibility for the accuracy, completeness, or usefulness, of any information, apparatus, product, or process disclosed, or represents that its use would not infringe privately owned rights. References herein to any specific commercial product, process, or service by trade name, trade mark, manufacturer, or otherwise, does not necessarily constitute or imply its endorsement, recommendation, or favoring by the U.S. Government or any agency thereof. The views and opinions of authors expressed herein do not necessarily state or reflect those of the U.S. Government or any agency thereof.

Microstructure characterization of electric field assisted sintering (EFAS) sintered metallic and ceramic materials using local thermal diffusivity measurement

Zilong Hua, Jorgen Fredrick Rufner, Arin Seth Preston, David H Hurley, Patrick Merighe, Spencer Doran, Robert Schley, Yuzhou Wang

September 2023




**Idaho National Laboratory
Idaho Falls, Idaho 83415**

<http://www.inl.gov>

**Prepared for the
U.S. Department of Energy
Under DOE Idaho Operations Office
Contract DE-AC07-05ID14517**

RESEARCH ARTICLE | SEPTEMBER 26 2023

Microstructure characterization of electric field assisted sintering (EFAS) sintered metallic and ceramic materials using local thermal diffusivity measurement

Zilong Hua ; Patrick Merighe ; Jorgen Rufner; Arin Preston; Robert Schley ; Yuzhou Wang; Spencer Doran; David Hurley 



AIP Advances 13, 095220 (2023)

<https://doi.org/10.1063/5.0160625>

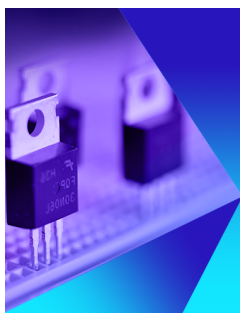


View
Online



Export
Citation

CrossMark



AIP Advances

Special Topic: Field Theory Methods in Condensed Matter Physics for Future Post-Transistor Devices

Submit Today



Microstructure characterization of electric field assisted sintering (EFAS) sintered metallic and ceramic materials using local thermal diffusivity measurement



Cite as: AIP Advances 13, 095220 (2023); doi: 10.1063/5.0160625

Submitted: 3 August 2023 • Accepted: 22 August 2023 •

Published Online: 26 September 2023



Zilong Hua,^{1,a)} Patrick Merighe,² Jorgen Rufner,¹ Arin Preston,¹ Robert Schley,¹ Yuzhou Wang,¹ Spencer Doran,³ and David Hurley¹

AFFILIATIONS

¹ Idaho National Laboratory, 1955 North Fremont Ave., Idaho Falls, Idaho 83415, USA

² Utah State University, 4130 Old Main Hill, Logan, Utah 84322, USA

³ Oregon State University, 1701 SW Western Blvd., Corvallis, Oregon 97331, USA

^{a)} Author to whom correspondence should be addressed: Zilong.hua@inl.gov

ABSTRACT

Electric Field Assisted Sintering (EFAS, also referred to as spark plasma sintering) is a powerful technology for the consolidation of powder materials. The high heating rate during the sintering process is critical for minimizing energy consumption, but it can also cause microstructure heterogeneities in sintered parts, such as spatially varied porosity. The examination of localized porosity usually requires the use of a scanning electron microscope with a carefully prepared surface. In this paper, photothermal radiometry is used to measure local thermal diffusivity and extract localized porosity of EFAS-sintered parts by using a percolation-threshold model. Applying this approach, we identified the radial position-dependent porosity variation in EFAS parts, which is likely formed due to the large temperature gradient during the sintering process. This approach has a unique advantage because it can measure samples with minimal or no surface preparation, enabling the possibility of *in situ* characterization in EFAS with proper system modification. Necessary modifications on the measurement approach for EFAS deployment and *in situ* characterization are also discussed.

© 2023 Author(s). All article content, except where otherwise noted, is licensed under a Creative Commons Attribution (CC BY) license (<http://creativecommons.org/licenses/by/4.0/>). <https://doi.org/10.1063/5.0160625>

I. INTRODUCTION

Electric Field Assisted Sintering (EFAS), also commonly referred to as Spark Plasma Sintering (SPS), is an advanced manufacturing technique for thermal processing of numerous material systems with good energy efficiency. It primarily uses metal and ceramic powders to rapidly consolidate them into dense parts or to bond them to bulk solid materials.^{1–5} During EFAS, a voltage bias is applied to the top and bottom rams between which the sample/tooling ensemble is located with uniaxial compression. Electrical current flows through percolation pathways in the graphite tooling with powders if the material is electrically conductive, or only in the graphite tooling if the material is an insulator. This generates heat throughout the sample/tooling ensemble via internal

resistive heating, allowing significantly more efficient heat transfer compared to similar technologies, i.e., hot pressing, hot isostatic pressing, or free sintering. Calculated from the reduced time to reach the desired temperature, energy savings from EFAS can be as high as 80%–90%.

It is challenging to sinter the part and reach the desired density. An *in situ* characterization tool to measure the density of the porous sample and monitor the density variation with a proper spatial resolution has long been due for the EFAS process. The single parameter available to infer sample consolidation in EFAS is the movement of the rams as the powder compact densifies. The ram movement can be correlated with the sample bulk density with the assumption that the sample is primarily shrinking in the direction of ram movement. Although valid in cylindrical,

disk shaped samples, this assumption does not work on samples that are net shaped and no longer radially symmetric. Tracking sample densification during manufacturing will need an *in situ* experimental approach for real time feedback, which remains a technical gap. Moreover, an unexpected local microstructure variation is reported in EFAS sintered parts, which is caused by the high heating rate (typically hundreds of degrees per minute) induced temperature gradients during sintering.⁶ The microstructure heterogeneities, such as the variations in density/porosity and grain size, may degrade the mechanical, thermal, optical, and electrical properties of the products.^{7,8} Meanwhile, under carefully designed sintering conditions, EFAS can be used to manufacture functionally graded materials with the desired microstructure variation.⁵ Currently, researchers can only rely on a trial-and-error approach to correlate EFAS sintering conditions with the microstructure of the final products, which combines the finite element modeling with time intensive, post-mortem analyses using a scanning electron microscope (SEM).^{9,10}

In this paper, we present our recent work on measuring local thermal diffusivity of EFAS sintered materials using photothermal radiometry (PTR), and we convert locally measured thermal properties to localized porosity using a mathematically simple percolation-threshold relation. Thermal transport is known to closely correlate with the microstructure. Typically, researchers focus on investigating how microstructure features, such as natural grain boundaries,^{11,12} irradiation induced damage,^{13–15} bonding interface,¹⁶ and larger-scale defect clusters and pores,¹⁷ influence thermal conductivity.¹⁸ The microstructure information is applied to predict and explain the thermal transport properties of advanced materials and their variations in different environments. Recently, successes have also been obtained from the reverse approach, i.e., exploring microstructure features by measuring thermal transport properties.^{19,20} For example, by measuring thermal transport properties combined with the lattice expansion from x-ray diffraction, Khafizov and co-workers quantified the point defect concentration in an ion-irradiated ceramic, which would otherwise be difficult by using advanced electron microscopes.²¹

In PTR measurements, an intensity-modulated laser is used to locally heat the sample and excite thermal waves, of which the propagation is probed by collecting blackbody radiation at different

locations.^{22–24} Thermal diffusivity can be extracted by comparing the thermal wave propagation with a continuous heat diffusion model.^{25,26} The PTR holds great promise for *in situ* microstructure characterization of EFAS sintered materials. As an optical approach, instrument deployment and remote measurements can be accomplished by using optical fibers. Different from other laser-based approaches, the PTR signal amplitude increases with emissivity, and thus, the measurement can be conducted on industrial grade surfaces that are not specially prepared. In addition, the blackbody radiation intensity, and thus the PTR signal level, increases nonlinearly with temperature, ideal for measurements in a high temperature environment, such as during sintering. Finally, the spatial resolution of PTR is tunable in the mesoscale range of 0.1–1 mm so that the experimental field of view can give accurate statistics with typical pore distributions found in EFAS parts.

We applied our methodology on identifying the porosity variation in EFAS parts, which was reported to be induced by the large temperature gradient during sintering.⁶ As the direction of such a temperature gradient depends on whether the sintered material is electrically conductive or not,²⁷ three materials were selected and sintered to different bulk densities for this study, with tungsten (W) serving as a model electrical conductor, alumina (Al_2O_3) as a model nonmetallic insulator, and boron carbide (B_4C) as a model semiconductor. The dependences of localized porosity on radial position are observed in all three sets of materials, especially on the ones with the lower bulk density. Random localized porosity variations were also revealed and located. With the ultimate purpose of developing the *in situ*, real-time monitoring capability of localized porosity variation for EFAS, necessary improvements in the measurement methodology are discussed.

II. METHODOLOGY

In PTR measurements, a laser beam (Blue Sky FTEC638-DHN01-01, with a wavelength of 638 nm and a peak power of 500 mW) with a periodically modulated intensity is focused on the sample surface to locally heat the sample. The resulting temperature field is probed by collecting blackbody radiation at different locations relative to heating using a pair of parabolic mirrors and a liquid-nitrogen cooled detector (Infrared Systems Development

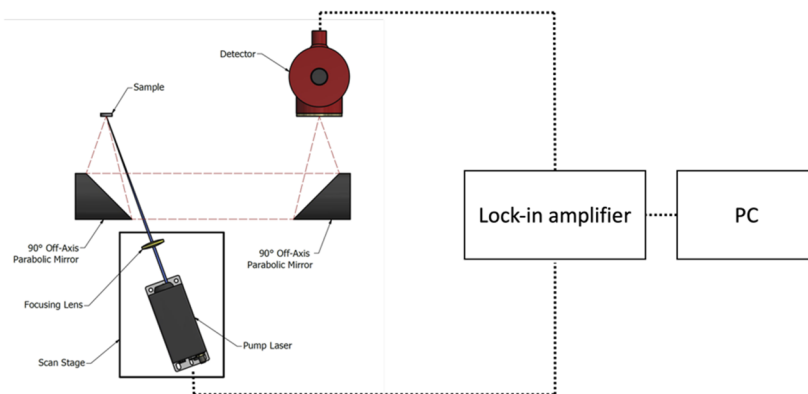


FIG. 1. A conceptual diagram of the PTR system.

MCT-13-0-0.25). As the analytical solution of the temperature field is a complex function and its amplitude is periodic in both spatial and temporal domains, this approach is called thermal wave measurement.²⁶ The thermal wave signal is analyzed using a lock-in amplifier (Stanford Research System SR830), and the phase information is used in a fitting process to extract thermal properties of interest.²⁵ The conceptual diagram of the PTR system is shown in Fig. 1, and the details of the measurement and system can be found in a previous publication.²⁴

The samples in this study were sintered by using a direct current sintering (DCS-5) system from Thermal Technology, LLC. The system can apply 5 tons of uniaxial force and 2000 amps of DC electrical current. The temperature is accurately controlled by proportional-integral-derivative (PID) with an optical pyrometer measurement input. All samples have a similar cylindrical geometry with a diameter of ~ 12 mm and thicknesses in the range of 2–5 mm. In each set, five samples with different bulk densities, ranging from highly porous to nearly 100% theoretical density, were sintered using empirically designed sintering procedures. The final bulk density values were measured in water via Archimedes' principle.²⁸ The samples were coarsely polished for PTR measurements to remove the graphite foil used during EFAS processing from pellet surfaces. After PTR measurements, the samples were finely polished using SiC papers and vibratory polishing for SEM characterization. The details of sample sintering conditions, density information, and surface preparation are given in the supplement material.

III. RESULTS

We first confirmed the qualitative correlation between local thermal diffusivity and local density. To avoid confusion, we define

“local density” as the density of the porous material at a specified area and “porosity” as the percentage of the pores in the material. Therefore, the mathematical correlation between local density, theoretical 100% density, and “localized porosity” exists as $\text{local density} = \text{theoretical 100\% density} \times (1 - \text{localized porosity})$. Three sets of local thermal diffusivity measurements were performed in the laser modulation frequency range of 1–200 Hz along different radial directions from the edge to the center on each sample. In order to distribute the measurement locations to cover more surface area, the direction of the first set of measurements was selected randomly, and the following sets were conducted in the direction rotated 90° counterclockwise from the previous one (sketch given as a part of Fig. 2). When measurements were conducted close to the edge (i.e., 1–1.5 mm, which is 2–3 times of the thermal diffusion length of the measurement), the semi-infinite boundary condition of the thermal wave solution would be violated, leading to an underestimation of the thermal diffusivity.²⁹ Therefore, the measurements were only conducted between $r = 0$ mm (center) and $r = 4$ mm, where r is the radial location. The separation between points is 1 mm. This limitation can be removed in future applications by using a more sophisticated data analysis. SEM characterization was conducted at the same locations of PTR measurements, and the local density was quantified from processing the SEM images using the open-source image processing software ImageJ. The details of the image processing can be found in the supplement material. Using 50%, 60%, and 100% dense Al_2O_3 samples as examples, we plot the normalized local densities (which equal the local density divided by theoretical 100% density, or $1 - \text{localized porosity}$) and normalized local thermal diffusivities (both normalized using the values at $r = 0$ mm) with respect to r in Fig. 2. A qualitative correlation between local thermal diffusivity and local density can be observed, as a higher density typically leads to a higher thermal diffusivity. Some outliers can be identified,

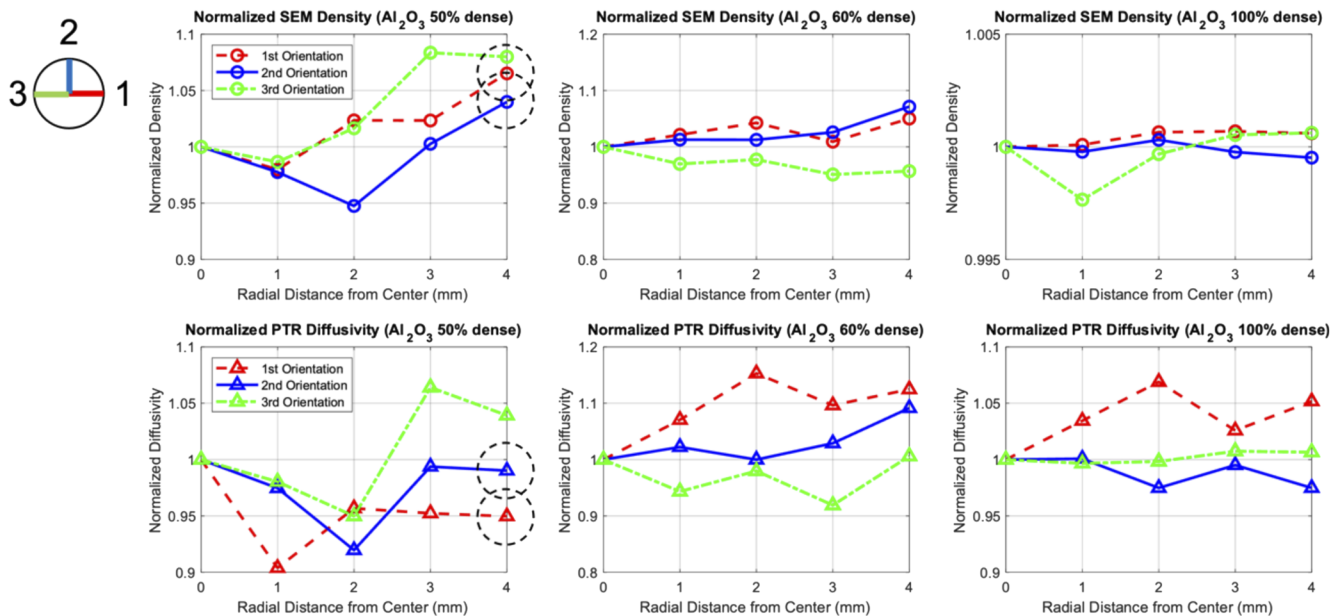


FIG. 2. Local density vs local thermal diffusivity with respect to radial locations (in three different directions, shown in different colors) on Al_2O_3 samples with densities of 50%, 60%, and 100%.

such as two data spots at $r = 4$ mm on 50% dense Al_2O_3 sample (highlighted in dash circles). The possible causes of the deviations are the uncertainties of image processing and PTR measurements (a few percent for both) and the resolution difference between PTR measurements (~ 0.5 mm) and SEM (~ 0.1 mm). In particular, as a thermal wave propagates in three dimensions, PTR measurements are sensitive to subsurface pores, which may not be seen in the two-dimensional SEM images.

Thermal conductivity–porosity correlations in porous materials have been investigated with several mathematical models suggested.^{30–37} We compared the models to identify the proper one to use in our work. As PTR measures thermal diffusivity, thermal conductivity (k) used in the models was converted to thermal diffusivity (D) using $D = k/\rho_0 c$, where ρ_0 is the theoretical 100% density and c is the specific heat. We also used the bulk properties to test the models to avoid the issues in local measurements, such as the resolution difference and underneath pores, as stated above. The bulk value of D was averaged from all measured local D in each sample, and the bulk porosity (ϕ) is converted from bulk density (ρ) measured using Archimedes' method and ρ_0 as $\phi = 1 - \rho/\rho_0$. For the convenient comparison among materials with different D , we further normalized D using the literature values of pore-free materials, as $D_r = D/D_0$, where D_r is the normalized thermal diffusivity and D_0 is the thermal diffusivity of the pore-free material. D_r can be found in the literature, or from the fully dense samples. D_r with respect to ϕ for all samples is shown in Fig. 3, with the lower (D_{LB}) and upper (D_{UB}) theoretical bounds suggested by Nikolopoulos and Ondracek³³ as

$$D_{LB} = (1 - \phi)^3, \quad (1)$$

$$D_{UB} = \frac{2(1 - \phi)}{2 + \phi}. \quad (2)$$

After comparing all existing analytical models in the literature,^{30–37} a mathematically simple “percolation-threshold relation”³² that only counts ϕ of the sample is found to work sufficiently well with

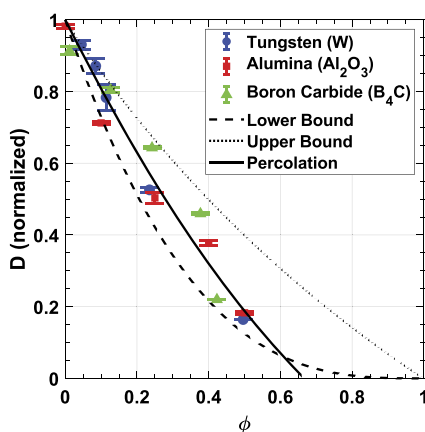


FIG. 3. Percolation model that quantitatively correlates normalized thermal diffusivity (D) with porosity (ϕ). The error bars give the standard error of bulk D , averaged from multiple sets of local D measurements.

comparable sensitivity and accuracy to, if no better than, the more complicated models that take parameters such as pore size and distribution into consideration.^{31,33} This is in agreement with the conclusion of Pabst and Gregorová in their review work.³² The percolation equation is given as

$$D_r = \left(1 - \frac{\phi}{2}\right) \left(1 - \frac{\phi}{\phi_c}\right), \quad (3)$$

where ϕ_c is the percolation threshold number. A value of $\phi_c = 2/3$ is used to represent spherical pores that are dominating in the samples in this study. This equation can be converted to solve for ϕ with measured D and pore-free D_0 as follows:

$$\phi = \frac{2D_0 + D_0\phi_c - 2\sqrt{\frac{D_0(4D_0 - 4D_0\phi_c + 8D\phi_c + D_0\phi_c^2)}{4}}}{2D_0}. \quad (4)$$

Equation (4) can be used to estimate both bulk and local ϕ (and calculate density) of EFAS sintered materials from PTR measurements. Equations (3) and (4) further suggest a nonlinear dependence of $D \propto \phi^2$. It can be translated to two perspectives. From the uncertainty perspective, this approach ensures a low uncertainty in the porosity estimation. As PTR measurement has a low uncertainty of 3%–5%,²⁴ the uncertainty of ϕ determined using this approach is calculated as 2%–3%. From the sensitivity perspective, it is expected that this approach is a more accurate estimation on ϕ than processing SEM images. Figure 2 shows that PTR results on the 60% and 100% dense Al_2O_3 samples have significantly larger variations between points than the ones from the image processing method. The largest difference on the 100% dense sample is up to 7% in PTR measurements (direction 1, represented in red) and is less than 0.3% in the image processing method (direction 3, represented in green). It is worth noting that this deviation is partly contributed by the resolution limitation of the image processing method. The statistical analysis across all images suggests that the number of small pores (diameter $< 2 \mu\text{m}$) is orders of magnitude higher than that of medium (diameter $= 2\text{--}14 \mu\text{m}$) and large pores (diameter $> 14 \mu\text{m}$). Pores with smaller diameters may be overlooked by the image processing software, leading to the underestimation of localized ϕ .

IV. DISCUSSION

Using Eq. (4), we examined the local density variation in EFAS parts induced by a temperature gradient. The density variation in the radial direction is shown in Fig. 4. The local density values along three different directions are averaged and normalized using the ones at $r = 0$ mm, with error bars representing the standard deviations. The results are divided into low-density group ($< 75\%$, upper panel in Fig. 4) and high-density group ($\geq 75\%$, lower panel in Fig. 4) for better presentation purposes. The results in Fig. 4 demonstrate the local density gradients in the radial direction in EFAS samples. As Nečina and Pabst *et al.* suggested,⁶ the trend of local density gradients (i.e., decreasing or increasing with r) is correlated with the temperature gradient during sintering, which ultimately correlates with the material electrical conductivity. For conductors such as W, the current goes through the sample powder during sintering and the temperature at the center is higher than at the edge, causing the

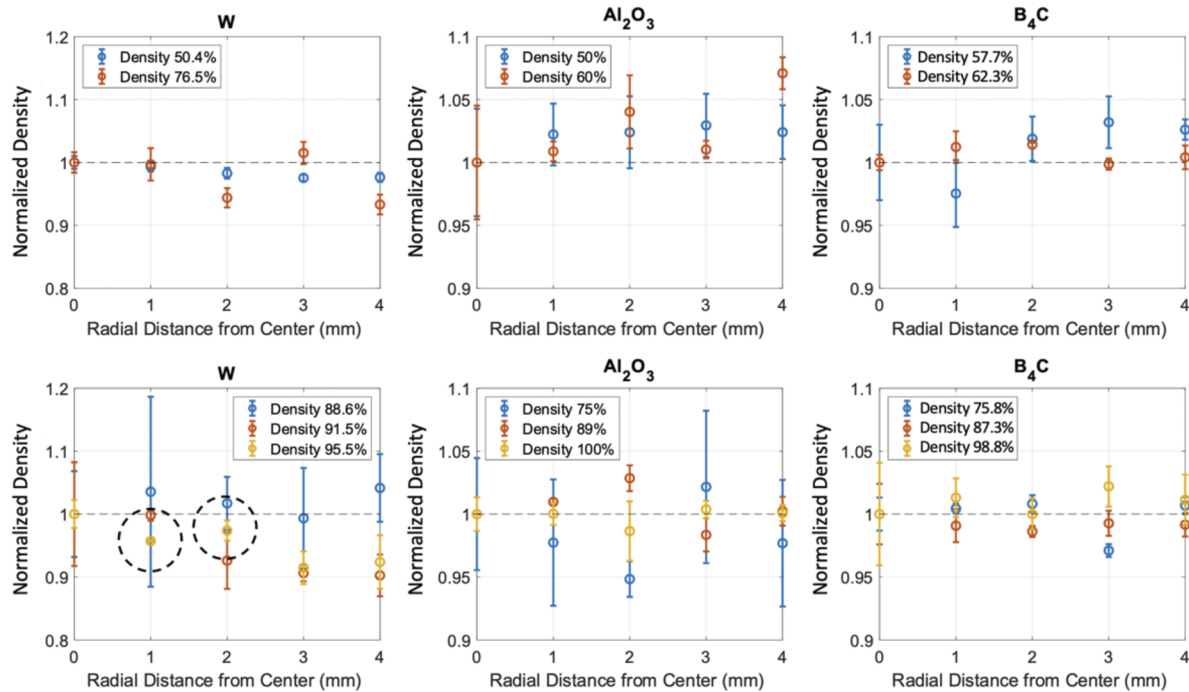


FIG. 4. Normalized local density at different radial locations. The general trend is that local density is higher at the center for conductors (represented by W) but at the edge for insulators (represented by Al_2O_3) and semiconductors (represented by B_4C).

local density higher at the center than at the edge as well. In contrast, in insulators, such as Al_2O_3 , and semiconductors, such as B_4C , the current goes around the powder (through the graphite tooling) during sintering, which leads to a higher temperature at the edge. Consequently, the density- r trend is reversed. Furthermore, as low-density samples have poorer thermal diffusivity, the heat dissipation is also slower, making the density variation more significant, and such a trend is more noticeable in the low-density group (upper panel in Fig. 4). All these findings evidence that the density variation was generated due to the temperature difference during the EFAS process.

Outliers (i.e., density with an unclear or opposite trend) were also found in some high-density set, such as 88.6% dense W, 75% Al_2O_3 , and 87.3% B_4C . The SEM images suggest that these outliers are due to “random” variations in the localized porosity. The dashed-circled data spots obtained on 95.5% dense W are used as an example. More pores can be seen in the SEM image at $r = 1$ mm, compared to the one at $r = 2$ mm (Fig. 5). These “random” localized porosity variations may be caused by other factors than the temperature difference, such as the lack of sufficient mixing of the powder or the imperfection of the tooling surface.

By using fibers to guide light and collect data, it is feasible to modify laser-based optical systems to deploy in closed space and conduct *in situ* characterization. Before making such a development on the PTR system to characterize localized porosity in real time during EFAS process, there are still questions to answer, and here, we list a few with possible solutions to our best knowledge. The first challenge is to reduce the excessive time required for data

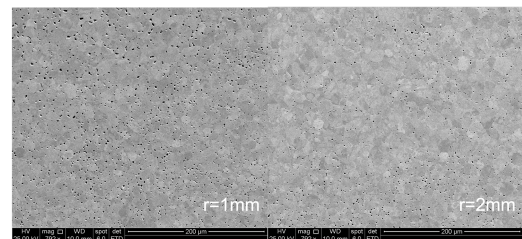


FIG. 5. SEM image comparison of the 95.5% dense W sample at two different locations. The local density at $r = 1$ mm is visibly lower than that at $r = 2$ mm, correctly captured by thermal property measurements.

collection. Current *ex situ* PTR measurements collect thermal wave phases at tens of locations with multiple modulation frequencies. Depending on the desired measurement accuracy, a set of data will take 5–90 min to collect, too long to serve as the real-time feedback. The possible solution is to perform PTR measurements in the time or frequency domain and only collect data at one location, or using fiber bundle with lock-in thermography. It can reduce the experiment time to a few minutes or shorter, with the trade-off of accuracy. Another challenge is that the analytical relation between thermal diffusivity and porosity is expected to change with temperature.³⁵ Using Eq. (4) suggested by our work to estimate density/porosity may introduce errors when applied at sintering temperatures. The solution is to repeat similar investigation as the one in this paper at different temperatures and set up a complete database. Moreover,

thermal transport may be influenced by other factors than porosity, such as phase transition. A better fundamental understanding on the sintered materials will be needed to separate the impacts on thermal transport from different factors.^{38,39}

V. CONCLUSION

In summary, in this study, we applied PTR to measure local thermal diffusivity across the surface of EFAS sintered materials and correlated it to localized porosity through an analytical percolation model. Using this approach, we confirmed the temperature gradient induced density variation in EFAS sintered materials. It can also be used to examine unexpected localized porosity, such as the ones from the lack of sufficient powder mixing or tooling imperfections. This work demonstrates the potential of using modified PTR systems for *in situ*, real-time density characterization of EFAS samples during the sintering process.

SUPPLEMENTARY MATERIAL

See the supplementary material for the details of sample sintering conditions to accomplish different bulk density, preparation steps for SEM imaging, and the image processing.

ACKNOWLEDGMENTS

This work was supported by the INL Laboratory Directed Research & Development (LDRD) Program under DOE Idaho Operations Office Contract No. DE-AC07-05ID14517, with the Project No. 22A-1059-142F.P.

AUTHOR DECLARATIONS

Conflict of Interest

The authors have no conflicts to disclose.

Author Contributions

Zilong Hua: Conceptualization (equal); Data curation (equal); Formal analysis (equal); Funding acquisition (equal); Investigation (equal); Methodology (equal); Project administration (equal); Software (equal); Supervision (equal); Validation (equal); Visualization (equal); Writing – original draft (equal); Writing – review & editing (equal). **Patrick Merighe:** Data curation (equal); Formal analysis (equal); Investigation (equal); Software (equal); Writing – original draft (supporting); Writing – review & editing (supporting). **Jorgen Rufner:** Project administration (supporting); Resources (lead); Writing – original draft (supporting). **Arin Preston:** Investigation (equal); Resources (equal); Writing – original draft (equal). **Robert Schley:** Methodology (supporting). **Yuzhou Wang:** Data curation (supporting); Formal analysis (supporting). **Spencer Doran:** Investigation (supporting); Resources (supporting). **David Hurley:** Conceptualization (supporting); Project administration (supporting); Supervision (supporting).

DATA AVAILABILITY

The data that support the findings of this study are available upon request from the corresponding author. The data are not publicly available due to state restrictions, such as privacy or ethical restrictions.

REFERENCES

- Y. S. Kim, T. W. Cho, and D.-S. Sohn, “Thermal conductivities of actinides (U, Pu, Np, Cm, Am) and uranium-alloys (U–Zr, U–Pu–Zr and U–Pu–TRU–Zr),” *J. Nucl. Mater.* **445**(1–3), 272–280 (2014).
- R. O’Brien and N. Jerred, “Spark plasma sintering of W–UO₂ cermets,” *J. Nucl. Mater.* **433**(1–3), 50–54 (2013).
- M. Samanta, K. Pal, U. V. Waghmare, and K. Biswas, “Intrinsically low thermal conductivity and high carrier mobility in dual topological quantum material, n-type BiTe,” *Angew. Chem., Int. Ed.* **59**(12), 4822–4829 (2020).
- R. V. R. Virtudazo *et al.*, “Improvement in the thermoelectric properties of porous networked Al-doped ZnO nanostructured materials synthesized via an alternative interfacial reaction and low-pressure SPS processing,” *Inorg. Chem. Front.* **7**(21), 4118–4132 (2020).
- C. L. Cramer, W. Li, Z.-H. Jin, J. Wang, K. Ma, and T. B. Holland, “Techniques for mitigating thermal fatigue degradation, controlling efficiency, and extending lifetime in a ZnO thermoelectric using grain size gradient FGMs,” *J. Electron. Mater.* **47**(1), 866–872 (2018).
- V. Nečina and W. Pabst, “Influence of the heating rate on grain size of alumina ceramics prepared via spark plasma sintering (SPS),” *J. Eur. Ceram. Soc.* **40**(10), 3656–3662 (2020).
- B.-N. Kim, K. Hiraga, K. Morita, and H. Yoshida, “Spark plasma sintering of transparent alumina,” *Scr. Mater.* **57**(7), 607–610 (2007).
- M. Prakasam, D. Michau, O. Viraphong, and A. Largeteau, “Optimal sintering parameters for Al₂O₃ optoceramics with high transparency by spark plasma sintering,” *Adv. Appl. Ceram.* **115**(6), 333–341 (2016).
- G. Guelou *et al.*, “Issues and opportunities from Peltier effect in functionally-graded colusites: From SPS temperature modeling to enhanced thermoelectric performances,” *Appl. Mater. Today* **22**, 100948 (2021).
- M. Nanko and K. Dang, “Two-step pulsed electric current sintering of transparent Al₂O₃ ceramics,” *Adv. Appl. Ceram.* **113**(2), 80–84 (2014).
- M. Khafizov *et al.*, “Thermal conductivity in nanocrystalline ceria thin films,” *J. Am. Ceram. Soc.* **97**(2), 562–569 (2014).
- Z. Hua, J. Spackman, and H. Ban, “Characterization of Kapitza resistances of natural grain boundaries in cerium oxide,” *Materialia* **5**, 100230 (2019).
- C. Jensen, M. Chirtoc, N. Horny, J. Antoniow, H. Pron, and H. Ban, “Thermal conductivity profile determination in proton-irradiated ZrC by spatial and frequency scanning thermal wave methods,” *J. Appl. Phys.* **114**(13), 133509 (2013).
- C. A. Dennett *et al.*, “The influence of lattice defects, recombination, and clustering on thermal transport in single crystal thorium dioxide,” *APL Mater.* **8**(11), 111103 (2020).
- W. R. Deskins *et al.*, “A combined theoretical-experimental investigation of thermal transport in low-dose irradiated thorium dioxide,” *Acta Mater.* **241**, 118379 (2022).
- D. H. Hurley, M. Khafizov, and S. Shinde, “Measurement of the Kapitza resistance across a bicrystal interface,” *J. Appl. Phys.* **109**(8), 083504 (2011).
- E. Gregorová, W. Pabst, Z. Sofer, O. Jankovský, and J. Matějček, “Porous alumina and zirconia ceramics with tailored thermal conductivity Journal of Physics: Conference Series,” *J. Phys.: Conf. Ser.* **395**(1), 012022 (2012).
- D. H. Hurley *et al.*, “Thermal energy transport in oxide nuclear fuel,” *Chem. Rev.* **122**(3), 3711–3762 (2021).
- C. A. Dennett *et al.*, “An integrated experimental and computational investigation of defect and microstructural effects on thermal transport in thorium dioxide,” *Acta Mater.* **213**, 116934 (2021).
- V. S. Chauhan, J. Pakarinen, T. Yao, L. He, D. H. Hurley, and M. Khafizov, “Indirect characterization of point defects in proton irradiated ceria,” *Materialia* **15**, 101019 (2021).

- ²¹M. Khafizov, J. Pakarinen, L. He, and D. H. Hurley, "Impact of irradiation induced dislocation loops on thermal conductivity in ceramics," *J. Am. Ceram. Soc.* **102**(12), 7533–7542 (2019).
- ²²L. Fabbri and P. Fenici, "Three-dimensional photothermal radiometry for the determination of the thermal diffusivity of solids," *Rev. Sci. Instrum.* **66**(6), 3593–3600 (1995).
- ²³J. Bisson and D. Fournier, "The coupled influence of sample heating and diffraction on thermal diffusivity estimate with infrared photothermal microscopy," *J. Appl. Phys.* **84**(1), 38–43 (1998).
- ²⁴Z. Hua, R. Schley, and D. Hurley, "Local measurement of bulk thermal diffusivity using photothermal radiometry," *Rev. Sci. Instrum.* **93**(4), 044903 (2022).
- ²⁵Z. Hua, H. Ban, M. Khafizov, R. Schley, R. Kennedy, and D. H. Hurley, "Spatially localized measurement of thermal conductivity using a hybrid photothermal technique," *J. Appl. Phys.* **111**(10), 103505 (2012).
- ²⁶A. Maznev, J. Hartmann, and M. Reichling, "Thermal wave propagation in thin films on substrates," *J. Appl. Phys.* **78**(9), 5266–5269 (1995).
- ²⁷E. A. Olevisky and L. Froyen, "Impact of thermal diffusion on densification during SPS," *J. Am. Ceram. Soc.* **92**, S122–S132 (2009).
- ²⁸P. Mohazzab, "Archimedes' principle revisited," *J. Appl. Math. Phys.* **05**(04), 836 (2017).
- ²⁹Z. Hua and H. Ban, "Thermal diffusivity measurement of focused-ion-beam fabricated sample using photothermal reflectance technique," *Rev. Sci. Instrum.* **88**(5), 054901 (2017).
- ³⁰S. Saraf, A. Singh, and B. G. Desai, "Estimation of porosity and pore size distribution from scanning electron microscope image data of shale samples: A case study on Jhuran formation of Kachchh Basin, India," *ASEG Ext. Abstr.* **2019**(1), 1–3.
- ³¹F. Ternero, L. G. Rosa, P. Urban, J. M. Montes, and F. G. Cuevas, "Influence of the total porosity on the properties of sintered materials—A review," *Metals* **11**(5), 730 (2021).
- ³²W. Pabst and E. Gregorová, "A new percolation-threshold relation for the porosity dependence of thermal conductivity," *Ceram. Int.* **32**(1), 89–91 (2006).
- ³³P. Nikolopoulos and G. Ondracek, "Conductivity bounds for porous nuclear fuels," *J. Nucl. Mater.* **114**(2–3), 231–233 (1983).
- ³⁴J. Liu, Y. Li, Y. Li, S. Sang, and S. Li, "Effects of pore structure on thermal conductivity and strength of alumina porous ceramics using carbon black as pore-forming agent," *Ceram. Int.* **42**(7), 8221–8228 (2016).
- ³⁵P. I. Pelissari, R. A. Angélico, V. R. Salvini, D. O. Vivaldini, and V. C. Pandolfelli, "Analysis and modeling of the pore size effect on the thermal conductivity of alumina foams for high temperature applications," *Ceram. Int.* **43**(16), 13356–13363 (2017).
- ³⁶X. Liu *et al.*, "The influence of pore size distribution on thermal conductivity, permeability, and phase change behavior of hierarchical porous materials," *Sci. China: Technol. Sci.* **64**(11), 2485–2494 (2021).
- ³⁷A. Wagh, "Porosity dependence of thermal conductivity of ceramics and sedimentary rocks," *J. Mater. Sci.* **28**(14), 3715–3721 (1993).
- ³⁸D. R. Brown, R. Heijl, K. A. Borup, B. B. Iversen, A. Palmqvist, and G. Snyder, "Relating phase transition heat capacity to thermal conductivity and effusivity in Cu₂Se," *Phys. Status Solidi RRL* **10**(8), 618–621 (2016).
- ³⁹G.-Y. Oh, Y.-K. Kim, S. K. Kim, H. K. Lim, and Y.-J. Kim, "Effects of grain size and texture on thermal conductivity of AZ31 during static recrystallization," *Mater. Trans.* **58**(8), 1241–1243 (2017).